AMERICAN SOCIETY FOR MICROBIOLOGY | Journal of Virology®

VIRUS-CELL INTERACTIONS

Molluscum Contagiosum Virus Protein MC008 Targets NF-κB Activation by Inhibiting Ubiquitination of NEMO

Thomas Phelan,[a] Clara Lawler,[a] Andreas Pichlmair,[b] Mark A. Little,[a] Andrew G. Bowie,[c] Gareth Brady[a]

[a]Trinity Health Kidney Centre, Trinity Translational Medicine Institute, Trinity College Dublin, St. James' Hospital Campus, Dublin, Ireland
[b]Max Plank Institute of Biochemistry, Martinsried, Germany
[c]School of Biochemistry and Immunology, Trinity Biomedical Sciences Institute, Trinity College Dublin, Dublin, Ireland

ABSTRACT Molluscum contagiosum virus (MCV) is a human-adapted poxvirus that causes a common and persistent yet mild infection characterized by distinct, contagious, papular skin lesions. These lesions are notable for having little or no inflammation associated with them and can persist for long periods without an effective clearance response from the host. Like all poxviruses, MCV encodes potent immunosuppressive proteins that perturb innate immune pathways involved in virus sensing, the interferon response, and inflammation, which collectively orchestrate antiviral immunity and clearance, with several of these pathways converging at common signaling nodes. One such node is the regulator of canonical nuclear factor kappa B (NF-κB) activation, NF-κB essential modulator (NEMO). Here, we report that the MCV protein MC008 specifically inhibits NF-κB through its interaction with NEMO, disrupting its early ubiquitin-mediated activation and subsequent downstream signaling. MC008 is the third NEMO-targeting inhibitor to be described in MCV to date, with each inhibiting NEMO activation in distinct ways, highlighting strong selective pressure to evolve multiple ways of disabling this key signaling protein.

IMPORTANCE Inflammation lies at the heart of most human diseases. Understanding the pathways that drive this response is the key to new anti-inflammatory therapies. Viruses evolve to target inflammation; thus, understanding how they do this reveals how inflammation is controlled and, potentially, how to disable it when it drives disease. Molluscum contagiosum virus (MCV) has specifically evolved to infect humans and displays an unprecedented ability to suppress inflammation in our tissue. We have identified a novel inhibitor of human innate signaling from MCV, MC008, which targets NEMO, a core regulator of proinflammatory signaling. Furthermore, MC008 appears to inhibit early ubiquitination, thus interrupting later events in NEMO activation, thereby validating current models of IκB kinase (IKK) complex regulation.

KEYWORDS molluscum contagiosum, MC008, human, innate, NEMO, NF-κB, ubiquitin, innate immunity, ubiquitination

Viruses and hosts coevolve over long periods of time, leading to constant selective pressure on both to refine the process of viral immune evasion, pitched against ever more effective ways of detecting and clearing viruses within the body. A crucial element of the innate immune response may be the vast repertoire of pattern recognition receptors (PRRs) expressed in a broad variety of cell types that detect distinct, conserved molecular structures known as pathogen-associated molecular patterns (PAMPs). These PRRs include Toll-like receptors (TLRs), retinoic acid-inducible gene I (RIG-I)-like receptors, and DNA sensors such as cyclic GMP-AMP synthase (cGAS) (1). The detection of PAMPs by PRRs activates signaling cascades that lead to the activation of nuclear factor kappa light chain enhancer of activated B cells (NF-κB) and interferon (IFN) regulatory factor (IRF) family transcription factors. Once activated and translocated into the nucleus,

Editor Derek Walsh, Northwestern University Feinberg School of Medicine

Address correspondence to Gareth Brady, BRADYG1@tcd.ie.

The authors declare no conflict of interest.

Received 20 January 2023
Accepted 17 February 2023
Published 14 March 2023

these transcription factors collaborate to induce proinflammatory cytokines and the expression of type I IFNs (2).

Following PRR and cytokine stimulation, signaling cascades that activate the canonical NF-κB pathway result in the activation of E3 ligase complexes. These complexes generate ubiquitin scaffolds that interact with NF-κB essential modulator (NEMO), the regulatory subunit of the IκB kinase (IKK) complex. This interaction enables the recruitment of the transforming growth factor β (TGF-β)-activated kinase 1 binding protein 2/3 (TAB2/3)–TGF-β-activated kinase 1 (TAK1) complex, which also binds these chains (3). NEMO is a 419-amino-acid protein composed of multiple domains, including two coiled-coil regions (CC1 and CC2) along with a leucine zipper (LZ) and a zinc finger (ZF), arranged into an elongated structure (4). The binding of NEMO to ubiquitin chains also induces a conformational change in NEMO. This exposes phosphorylation sites on IKKα and IKKβ, thus enabling the phosphorylation of IKKβ by proximal TAK1 during canonical NF-κB signaling (5). IKKβ phosphorylates the NF-κB p65 subunit and IκBα, an inhibitory protein that is constitutively bound to NF-κB in the cytoplasm. The proteasomal degradation of IκBα induced by phosphorylation releases phosphorylated NF-κB, which can then translocate into the nucleus where it transactivates proinflammatory and antiviral gene expression (6).

Consequently, viruses evolve to suppress and evade the activation of these pathways (7–9). Poxviruses are particularly adept at this and have evolved a wide spectrum of immunoregulators that bind host proteins, disrupting inflammation and the antiviral immune response (8, 9). Molluscum contagiosum virus (MCV) is a common cause of dermatropic infection resulting in the formation of papular lesions that can persist in the epidermis for months and even years in some cases (10). MCV is the only known, extant poxvirus that appears to have specifically adapted to human infection. Of the 182 proteins predicted to be encoded by the MCV genome, MCV has 105 orthologs in other orthopoxviruses, many of which appear to be unique (11). In recent years, much progress has been made in identifying immunoregulators encoded by the MCV genome. These include MC005 (12), MC080 (13), MC132 (14), MC159 (15, 16), and MC160 (17), with many more likely remaining to be discovered given the known densities of these inhibitors in well-studied poxviruses (7, 9).

Thus, while much of the research into poxvirus immune evasion to date has revolved around other members of the poxvirus family, most of the MCV genome remains to be extensively investigated. Furthermore, understanding innate immune antagonists encoded by this human-adapted poxvirus may provide valuable insights into previously unknown facets of human innate immune signaling pathways and perhaps highlight novel targets for therapeutic intervention in disease. We previously reported that MC005 targets a key control point in NF-κB activation by binding to NEMO after activation and prevents "conformational priming" (12). Here, we report that the MCV protein MC008 inhibits human NF-κB activation at an earlier point than MC005 by disrupting NEMO monoubiquitination, which consequently impacts later activation events. Heavy genetic investment in targeting key signaling control nodes is common in poxviruses (12, 16, 18–22), highlighting the importance of these regulatory proteins in antiviral signaling and perhaps the key role of NEMO in antiviral responses against MCV.

RESULTS

MC008 inhibits NF-κB activity induced by cytosolic nucleic acid sensing and antiviral Toll-like receptors. We screened a library of MCV open reading frames (ORFs) for their ability to inhibit inflammatory signaling using a high-throughput luciferase assay-based screening system and identified MC008 as an inhibitor of NF-κB activation for further investigation (data not shown). MC008 is a 176-amino-acid protein (predicted molecular mass, 19 kDa) with an ORF located in the left-hand terminus of the MCV genome.

We generated a tetracycline-inducible stable MC008-expressing line using HeLa cells that possess a DNA-sensing system (23). MC008 expression was induced and

subsequently detected in these cells (Fig. 1A). Interleukin-6 (IL-6) levels were measured in both induced and uninduced cells following stimulation by transfection with poly (dA-dT), and MC008 expression was correlated with a significant decrease in IL-6 release (Fig. 1B). Confocal analysis revealed that MC008 localizes throughout HEK293T cells, with strong staining in the nucleus (Fig. 1C).

We next employed a luciferase assay-based screen driving pathway activation with ligands or overexpressing key elements of signaling pathways to simulate activation at distinct points and parsing the effects on activation using NF-κB and ISRE (interferon-stimulated response element) (IRF-inducible) reporters. We previously observed that MC020 had no effects on any innate pathways investigated in early MCV genome screens (data not shown), and it was thus used as a negative-control MCV protein in our analyses. Both the MC008 and MC020 proteins were expressed at approximately equivalent levels (Fig. 1D).

The cGAS-STING (stimulator of interferon genes) pathway, a key DNA-sensing pathway, can be reconstituted in HEK293T cells by coexpressing the constructs for cGAS and STING, as they are not usually detectable in these cells (24). While MC008 expression potently inhibited the activation of NF-κB by this system, it had no effect on cGAS-STING-induced IRF activation (ISRE and IRF3-GAL4 reporters) (Fig. 1E to G). The RIG-I pathway has been reported to be an indirect poxvirus DNA-sensing system in HEK293T cells, enabled by the presence of RNA polymerase III, which transcribes AT-rich DNA into an RNA ligand (25). As such, both poly(dA-dT) stimulation and mitochondrial antiviral-signaling protein (MAVS) expression were used as activators of the RIG-I signaling pathway. As with DNA sensing signaling, MC008 was unable to inhibit the activation of ISRE by this pathway but potently inhibited NF-κB activation (Fig. 1H to J). We next examined the effect of virus-induced IFN-β promoter activity, which is both NF-κB and IRF dependent, and observed that Sendai virus-induced IFN-β signaling in HEK293T cells was impaired (Fig. 1K).

Next, we examined the effect of MC008 on TLR-driven signaling by overexpressing a constitutively active CD4 fusion of TLR3 and two downstream adaptor proteins used in TLR signaling, its adaptor TRIF and MyD88, an adaptor utilized by several TIR domain-containing receptors like TLR4 (26). Consistent with our other observations, MC008 inhibited NF-κB activity in CD4TLR3-, MyD88-, and TRIF-driven signaling (Fig. 1L to N). While TRIF activates both NF-κB and ISRE, MC008 was again unable to inhibit the ISRE-activating arm of the response (Fig. 1O). Together, these data suggested that MC008 is a specific inhibitor of NF-κB activation and targets a downstream point common to all innate sensing pathways that we investigated.

MC008 inhibits NF-κB activation induced by proinflammatory cytokines. While the upregulation of type I interferons is key for the antiviral response, the upregulation of proinflammatory cytokines is another crucial aspect of antiviral immunity. Inflammation triggers the presence of infection in the wider immune system, linking innate and adaptive immunity through the activation and recruitment of various immune cells to facilitate the emergence of a specific adaptive response (9). After we determined that MC008 specifically inhibits NF-κB activation without affecting IRF activation by upstream elements of nucleic acid-sensing pathways, we next investigated whether NF-κB activity induced by proinflammatory cytokines was similarly inhibited.

We stimulated inducible MC008 stable HeLa cells with tumor necrosis factor alpha (TNF-α) and again found a significant decrease in IL-6 release (Fig. 2A). We then measured NF-κB activation in HEK293T cells and found that MC008 inhibited NF-κB activity driven by IL-1β and TNF-α (Fig. 2B and C). To further investigate where in these pathways MC008 was exerting its effect, we next examined the effect of MC008 on signaling induced by the E3 ligases TRAF2 (TNF receptor-associated factor 2) and TRAF6, which play key regulatory roles in TNF- and IL-1/TLR/sensing pathway-activated signaling, respectively (27). Again, in line with our previous observations, MC008, but not the control protein MC020, inhibited NF-κB activation (Fig. 2D and E). The specificity of MC008 inhibition of NF-κB signaling was further indicated by the lack of inhibition of

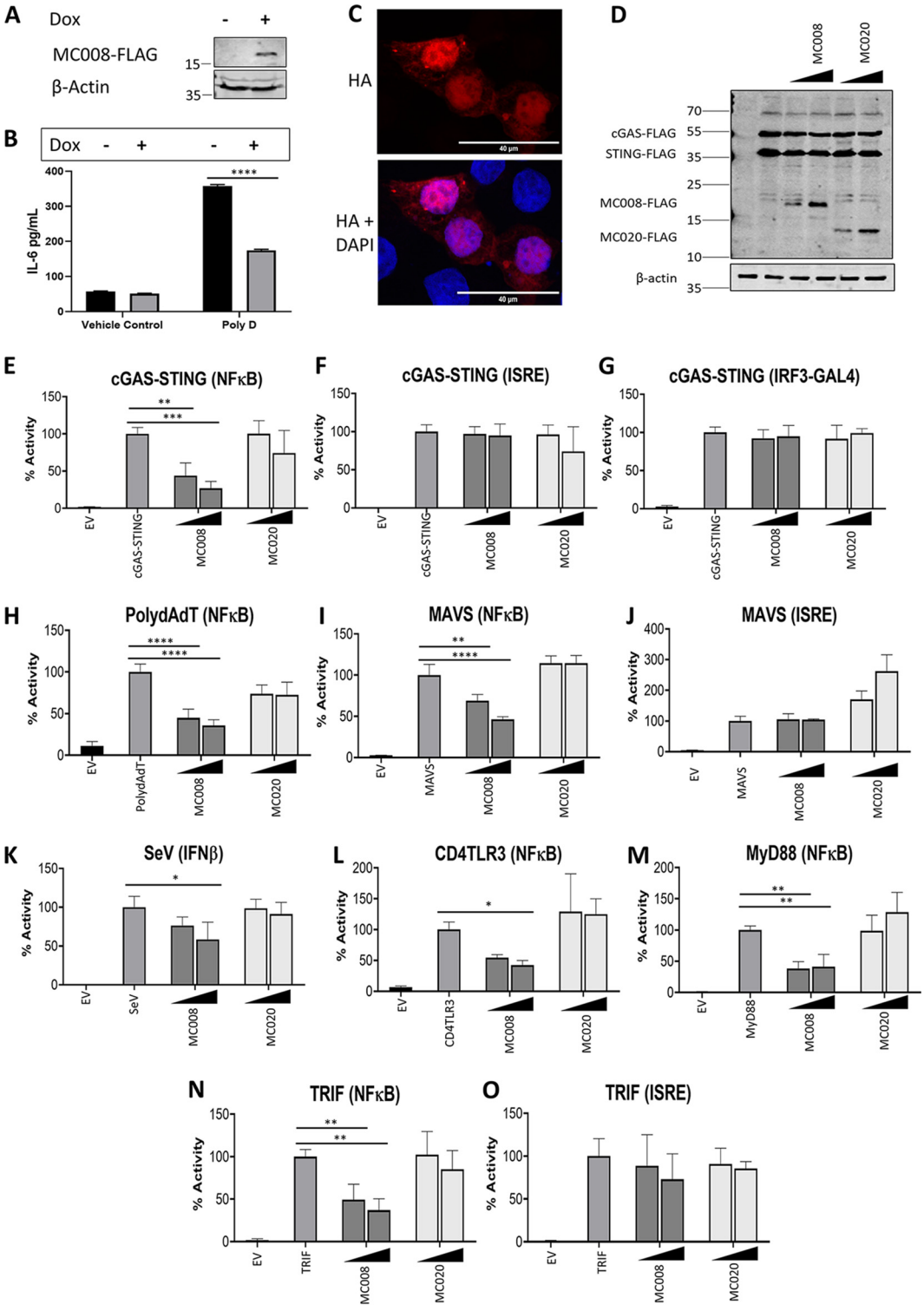

FIG 1 MC008 inhibits the cytosolic nucleic acid-sensing pathway and antiviral TLR activation of NF-κB. (A) HeLa cells were transduced with lentivirus containing Lenti-X Tet-One inducible MC008-FLAG. Following selection, 3×10^5 cells/well were seeded into a 6-well plate and were left untreated (−) or stimulated with 100 ng/mL of doxycycline (Dox) (+) for 24 h to stimulate MC008 expression. Cells were subsequently lysed 24 h later, followed by immunoblotting. (B) A total of 1×10^5 stable HeLa cells/mL were transfected with 1 μg/mL poly(dA-dT) for 24 h following MC008 induction. Serum-free medium and Lipofectamine 2000 were used as the vehicle control. The cell supernatants were subsequently harvested, and IL-6 levels were measured using an ELISA. (C) Localization of MC008 in HEK293T cells. Cells were transfected with 100 ng of the pCEP4-MC008-HA expression vector and fixed 24 h later. Cells were subsequently stained with DAPI (blue) or probed with anti-HA (red). (D) HEK293T cells were seeded at 2×10^5 cells/mL and transfected with 80 ng of NF-κB and 40 ng of

(Continued on next page)

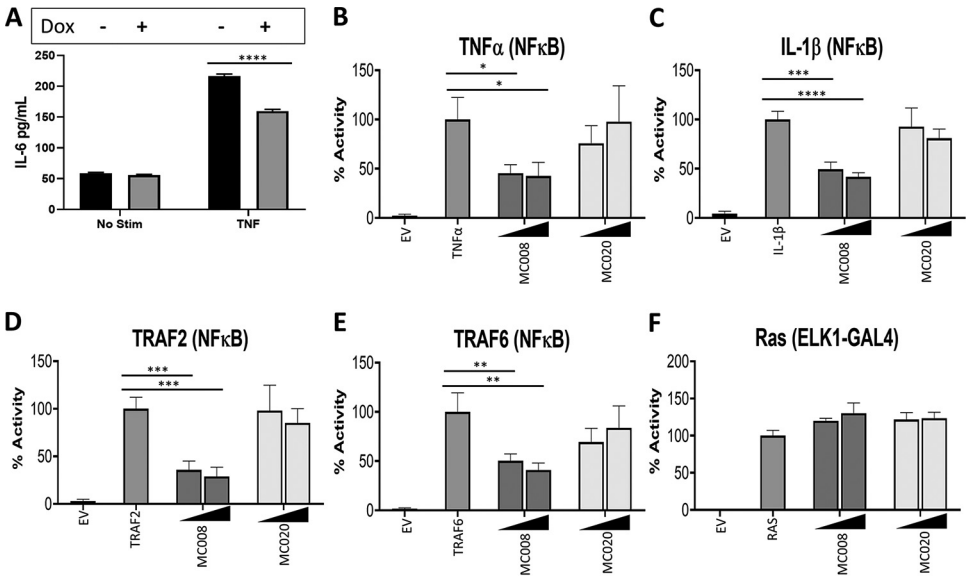

FIG 2 MC008 inhibits TNF-α- and IL-1β-stimulated NF-κB activation. (A) A total of 1×10^5 stable HeLa cells/mL were stimulated with 50 ng/mL of TNF-α for 24 h following MC008 induction with doxycycline, and IL-6 levels were measured using an ELISA. (B and C) Effect of MC008 on TNF- and IL-1-stimulated NF-κB activation. A total of 2×10^5 cells/mL were transfected with 80 ng of the NF-κB reporter gene and 40 ng of the thymidine kinase promoter-Renilla luciferase (TK *Renilla*) reporter gene, along with 25 or 50 ng of the MCV ORFs indicated, for 24 h. Cells were then stimulated with 50 ng/mL TNF-α or IL-1β for 8 h, subsequently lysed, and assayed for NF-κB reporter activity. (D and E) Similar to panels B and C except that 50 ng of TRAF2 and TRAF6 was overexpressed to drive NF-κB signaling. (F) The activation of Elk1 by Ras was measured by transfecting 80 ng of the pFR-luciferase reporter along with 50 ng of Ras, 5 ng of pFA-Elk1, and the indicated MCV ORFs (25 and 50 ng). Data are presented as percentages of reporter activation compared to the positive control and are the combined means ± standard deviations for triplicate samples from representative experiments ($n = 3$). Statistical significance is indicated by asterisks (*, $P < 0.05$; **, $P < 0.01$; ***, $P < 0.001$; ****, $P < 0.0001$).

the Ras-Elk1 mitogenic signaling pathway where RasVHa activation of Elk1 is monitored using an Elk1-GAL4 DNA binding domain fusion that induces a GAL4 promoter luciferase system (Fig. 2F).

MC008 inhibits NF-κB activation at the level of the IKK complex. Due to the ability of MC008 to inhibit a wide range of pathways and stimuli that induce NF-κB (Fig. 3A), this suggested that MC008 exerts its effects at a point common to all of these pathways. We investigated the effect of MC008 on the IKK complex, now including two inhibitors that we previously identified, MC005 (which inhibits NEMO activation) and MC132 (which drives NF-κB p65 degradation), as inhibitory reference points (12, 14). TAB2 operates proximal to the IKK complex and functions as a ubiquitin binding adaptor protein required for the recruitment of TAK1 (3). We observed that MC008, MC005, and MC132 inhibited NF-κB activity following the expression of TAB2 (Fig. 3B). The ectopic expression of wild-type NEMO does not drive signaling, presumably due to the absence of the ubiquitin-induced conformational change required to activate downstream signaling. Thus, we used a constitutively active K277A mutant form of NEMO that simulates the active state of NEMO after ubiquitin-mediated activation to drive NF-κB at this pathway point (12, 28). All three inhibitors potently inhibited NF-κB activation by the NEMO K277A mutant (Fig. 3C).

FIG 1 Legend (Continued)
the TK *Renilla* reporter gene, along with the empty vector and 25 or 50 ng of MC008-FLAG and MC020-FLAG for 24 h. Cell lysates were subsequently harvested, and Western blotting was performed. (E to O) Similarly, HEK293T cells were seeded at 2×10^5 cells/mL and transfected as follows: 80 ng of NF-κB luciferase and 40 ng of TK Renilla reporter genes; 50 ng of the pathway activators TAB2, NEMO K277A mutant or IKKα; or 10 ng of IKKβ, or 1 ng of p65; 25 or 50 ng of the indicated MCV ORFs; and the final volume was adjusted to 220 ng with empty vector. 25 ng of cGAS and 25 ng of STING; 10 ng of MAVS; 5 ng of IRF3-GAL4; 50 ng of MyD88, CD4TLR3, or TRIF; 1 μg/mL of poly(dA-dT); or Sendai virus (SeV) was used to activate the pathways. The cells were subsequently lysed after 24 h and assayed for NF-κB and ISRE, IRF3-GAL4, or IFN-β reporter activity. Data are presented as percentages of reporter activation compared to the positive control and are the combined means ± standard deviations for triplicate samples from representative experiments ($n = 3$). Statistical significance is indicated by asterisks (*, $P < 0.05$; **, $P < 0.01$; ***, $P < 0.001$; ****, $P < 0.0001$).

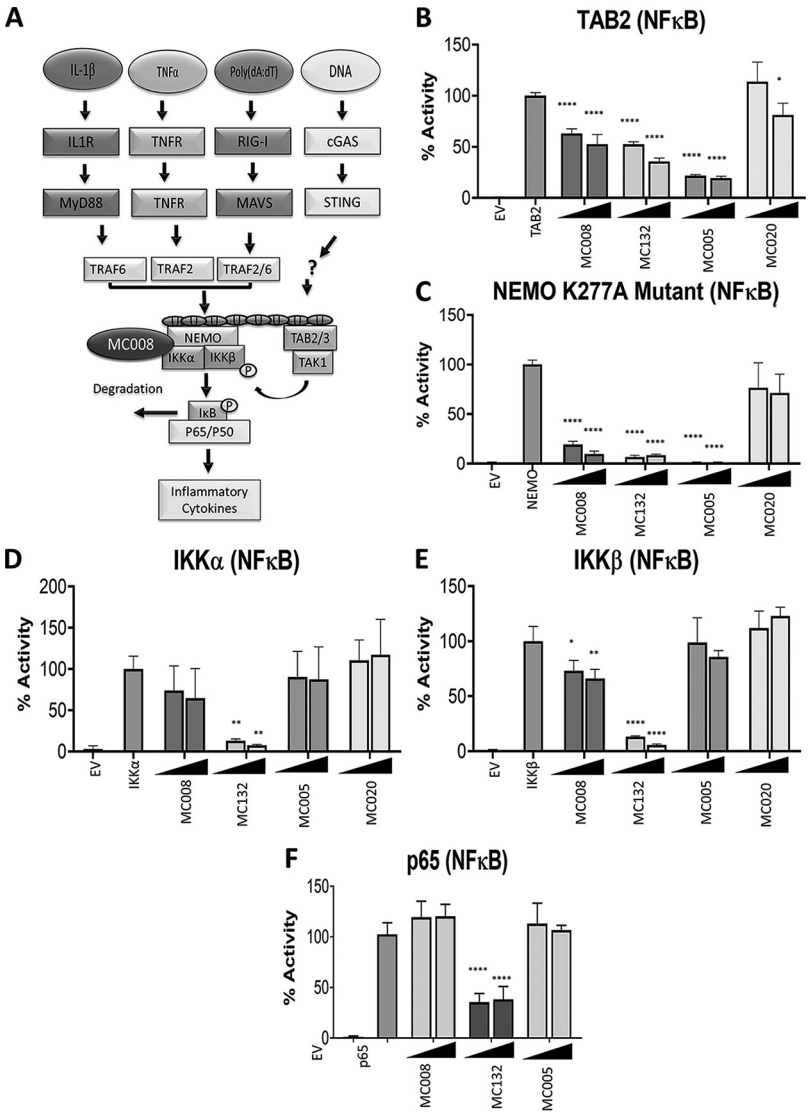

FIG 3 MC008 inhibits at a point proximal to the IKK complex. (A) Schematic showing multiple signaling pathways involved in NF-κB activation expected to be triggered by poxvirus infection. All of these pathways are perturbed by MC008 expression, as demonstrated above. IL1R, interleukin-1 receptor; TNFR, tumor necrosis factor receptor. (B to F) Comparison of MC008, MC005, and MC132 inhibition of signal transduction surrounding IKK complex activation. HEK293T cells were seeded at 2×10^5 cells/mL and transfected as follows: 80 ng of NF-κB luciferase and 40 ng of TK *Renilla* reporter genes; 50 ng of the pathway activators TAB2, NEMO K277A mutant or IKKα; or 10 ng of IKKβ, or 1 ng of p65; 25 or 50 ng of the indicated MCV ORFs; and the final volume was adjusted to 220 ng with empty vector. The cells were subsequently lysed after 24 h and assayed for NF-κB reporter activity. Data are presented as percentages of reporter activation compared to the positive control and are the combined means ± standard deviations for triplicate samples from individual experiments ($n = 3$). Statistical significance is indicated by asterisks (*, $P < 0.05$; **, $P < 0.01$; ***, $P < 0.001$; ****, $P < 0.0001$).

However, when we activated the system with IKKα and IKKβ, the inhibitory effects of MC008 and MC005 on NF-κB activity were greatly diminished, while MC132 inhibition was maintained (Fig. 3D and E). This indicated that inhibition by MC008, similar to MC005, was at a level proximal to NEMO, unlike MC132, which targets NF-κB p65 downstream. Likewise, MC008 and MC005 inhibition was similarly bypassed by driving signaling with small amounts of p65, whereas MC132 still retained the capacity to inhibit its direct target protein (Fig. 3F). Thus, these data indicated that MC008, like MC005, exerted its inhibitory activity at the level of the IKK complex, most likely by targeting NEMO.

MC008 interacts with NEMO. To confirm that MC008 was targeting NEMO at the level of the IKK complex, we first investigated MC008 coimmunoprecipitation with the

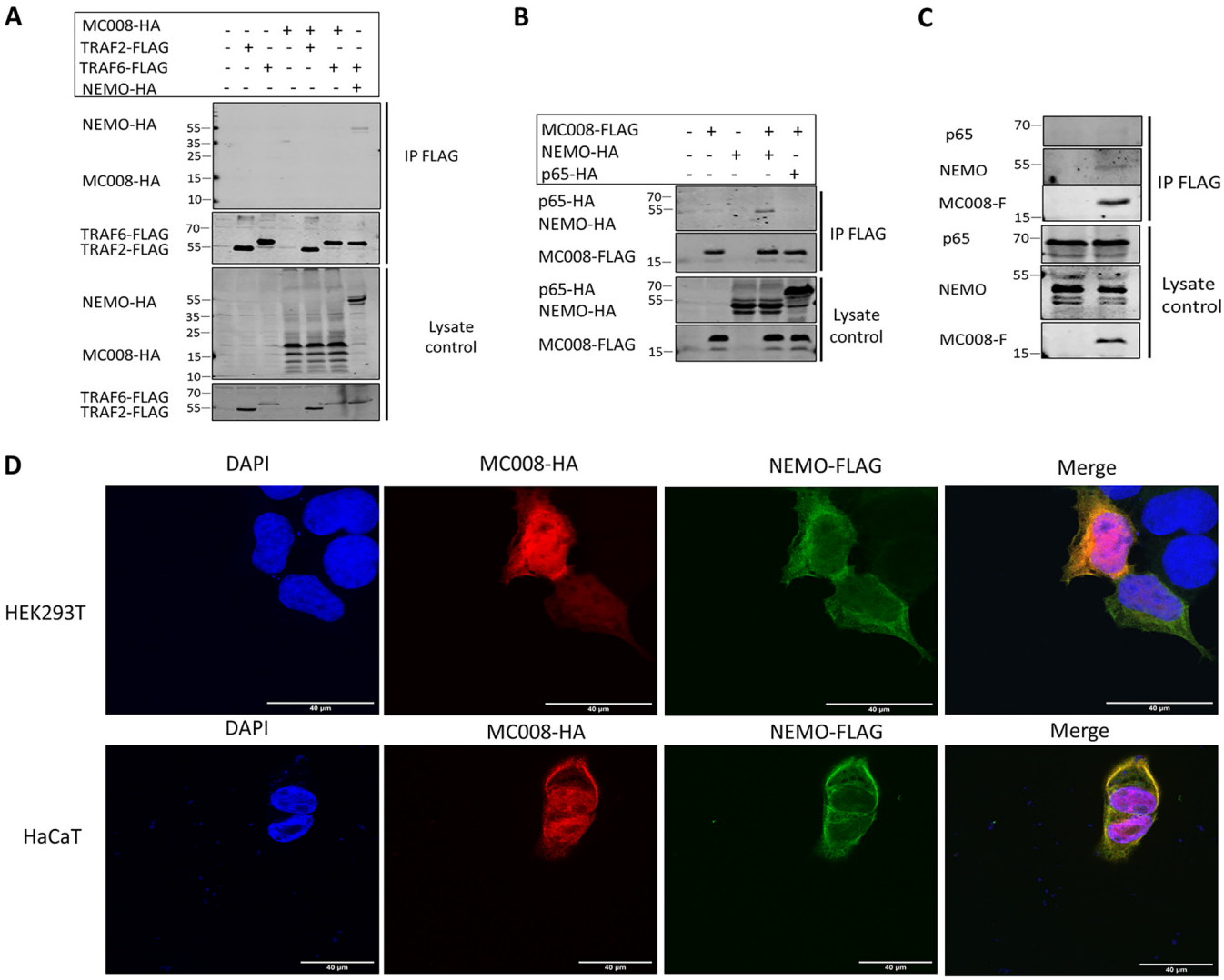

FIG 4 MC008 interacts with NEMO. (A and B) Four micrograms of MC008 and 4 μg of the indicated signaling elements were transiently expressed in 4×10^6 HEK293T cells per plate. The cells were subsequently lysed using ice-cold lysis buffer with a cocktail of phosphatase and protease inhibitors, and coimmunoprecipitation (IP) was performed. The resulting immunoprecipitants were then immunoblotted with the antibodies indicated. Representative blots (n = 3) are shown. (C) A total of 2×10^6 HaCaT cells per plate were transiently transfected with 4 μg of MC008 but not NEMO. Coimmunoprecipitation was performed, and the interaction with endogenous levels of NEMO was confirmed using a NEMO-specific antibody during immunoblotting. An antibody against endogenous p65 was used as a negative control for the pulldown. (D) HEK293T and HaCaT cells were seeded at 70,000 and 30,00 cells per well in 8-well chamber slides, respectively. Twenty-four hours later, they were transfected with 100 ng of expression vectors for MC008-HA and NEMO-FLAG. Cells were then fixed 24 h later and stained with DAPI (blue), FLAG (green), and HA (red).

signaling components TRAF2 and TRAF6. We observed that while NEMO was able to interact with TRAF6, as expected, no interaction between MC008 and TRAF2 or TRAF6 was detected (Fig. 4A). Conversely, we observed a strong interaction between NEMO and MC008 but no interaction between MC008 and p65, which lies downstream of the IKK complex (Fig. 4B). Using MC008 transiently expressed in HaCaT cells, we confirmed this interaction with endogenous NEMO but observed no association of MC008 with endogenous p65 (Fig. 4C). Furthermore, even though MC008 is predominantly nuclear, we observed enrichment in areas of the cytoplasm expressing NEMO using confocal microscopy, demonstrating colocalization in both HEK293T and HaCaT cells (Fig. 4D). These data suggested that MC008 was directly targeting NEMO.

MC008 inhibits NEMO ubiquitination. To identify the region of NEMO required for the MC008 interaction, we employed truncations corresponding to the functional domains of NEMO that we generated in previous work (12) and investigated their ability to interact with full-length MC008 (Fig. 5A and B). Interestingly, the MC008 association

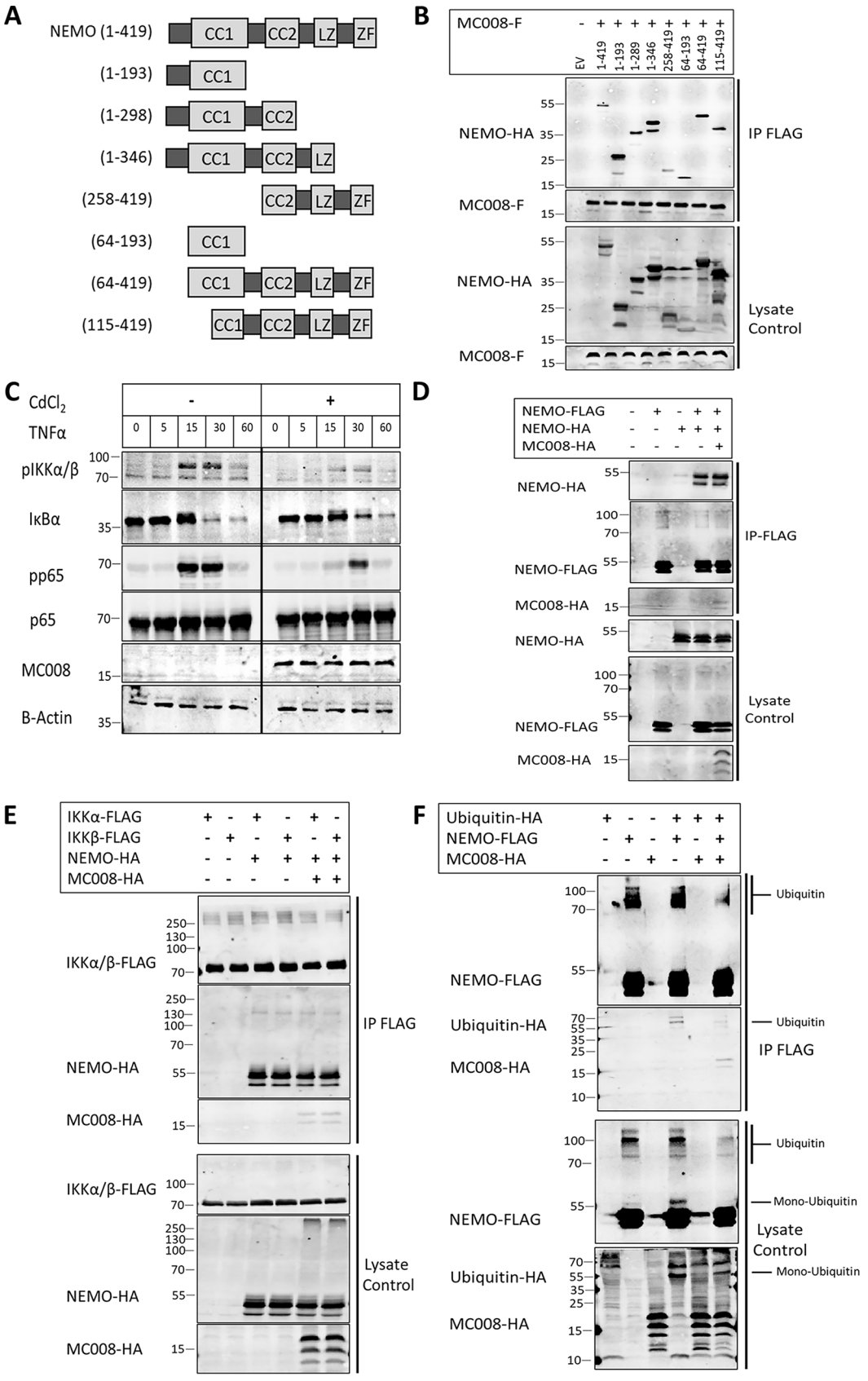

FIG 5 MC008 disrupts NEMO ubiquitination. (A) NEMO truncations were generated according to the schematic. (B) Four micrograms of MC008-FLAG and 4 μg of NEMO or the indicated truncations were transiently expressed in 4 $\times$ 10^6

(Continued on next page)

was maintained to various extents across all NEMO truncations. However, there was a notably reduced association with the truncation spanning positions 258 to 419, a region lacking the CC1 domain, indicating that this region is important for the interaction with MC008 and that, unlike MC005, this viral protein likely interacts with more than one region of NEMO.

To probe the consequences of inhibition at the point of NEMO, we examined the effect of MC008 binding to NEMO on downstream signaling elements by stimulating inducible MC008 stable HEK293T cells with TNF-α. We examined the phosphorylation of IKKα/β and p65 along with IκBα degradation, events that are known to be necessary for NF-κB activation. Interestingly, while MC008 inhibited IKKα/β and p65 phosphorylation, it caused only a slight but consistent delay during the course of IκBα degradation at 30 min (Fig. 5C).

We next investigated the mechanism of MC008 inhibition of NEMO. First, we examined the effect of MC008 on NEMO oligomerization by immunoprecipitation with FLAG- and hemagglutinin (HA)-tagged NEMO. The IKK complex unit is believed to consist of four NEMO molecules and two molecules each of IKKα/β, which are constitutively assembled even in the absence of upstream signaling (29). We observed no difference in the ability of NEMO to oligomerize when MC008 was introduced, suggesting that MC008 does not interfere with NEMO assembly within the IKK complex (Fig. 5D). We then examined whether MC008 was perturbing interactions between NEMO and IKKα/β, which are indispensable components of the multimeric IKK complex. Again, we observed no effect on the association of NEMO and the IKKs (Fig. 5E).

Given the central role of ubiquitination in NEMO activation, we next examined the effect of MC008 on its regulation by ubiquitin. We observed both monoubiquitination and polyubiquitination of NEMO when ubiquitin was overexpressed (Fig. 5F). These are key modifications in NEMO activation (5, 30, 31), with initial monoubiquitination being shown to be required for further polyubiquitination (32, 33). Interestingly, MC008 disrupted both forms of ubiquitin (Fig. 5F). Thus, these data suggest that MC008 inhibits NF-κB signaling by preventing the monoubiquitination and, thus, the polyubiquitination of NEMO, key regulatory steps required for downstream signaling. This notably differs from MC005, which does not affect NEMO ubiquitination or the association with ubiquitin chains but instead inhibits conformational changes in NEMO required for IKK phosphorylation (12).

Taken as a whole, these data indicate that MC008 specifically inhibits NF-κB activation by preventing the early ubiquitination of NEMO in all innate signaling pathways that we tested, thereby inhibiting the phosphorylation of IKK proteins with specific effects on subsequent NF-κB activation (Fig. 6). Given that at least three MCV proteins appear to target NEMO in distinct ways (Table 1), this is indicative of the importance of NEMO in antiviral immunity against this virus.

DISCUSSION

Poxvirus immune evasion research to date has largely centered around orthopoxviruses, particularly vaccina virus (9, 34). The molluscipoxvirus MCV is an understudied yet globally endemic human-specific poxvirus that causes a clinically mild infection in immunocompetent individuals, forming distinct papular skin lesions of long duration (35). The typical absence of inflammation around these lesions is different from other

FIG 5 Legend (Continued)
HEK293T cells per plate. The cells were subsequently lysed, and coimmunoprecipitation was performed. The resulting immunoprecipitants were then immunoblotted with anti-FLAG and anti-HA antibodies. A representative blot ($n = 3$) is shown. (C) HEK293T cells, stably expressing pMEP4-MC008-FLAG, were seeded at 6×10^5/well into six-well dishes and were left untreated (−) or treated with 1 μm $CdCl_2$ to induce MC008 expression (+). Cells were stimulated 24 h later with 50 ng/mL of TNF-α for the times indicated, and lysates were immunoblotted with the antibodies indicated. A representative blot ($n = 3$) is shown. (D to F) The indicated proteins were transiently expressed in 4×10^6 HEK293T cells per plate in the following ratios: 2 μg of NEMO-FLAG, 2 μg of NEMO-HA, 3 μg of IKKα-FLAG or IKKβ-FLAG, 1 μg of ubiquitin-HA, and 3 μg of MC008-HA. The cells were subsequently lysed, and coimmunoprecipitation was performed. Black lines indicate areas of ubiquitination. Representative blots ($n = 3$) are shown.

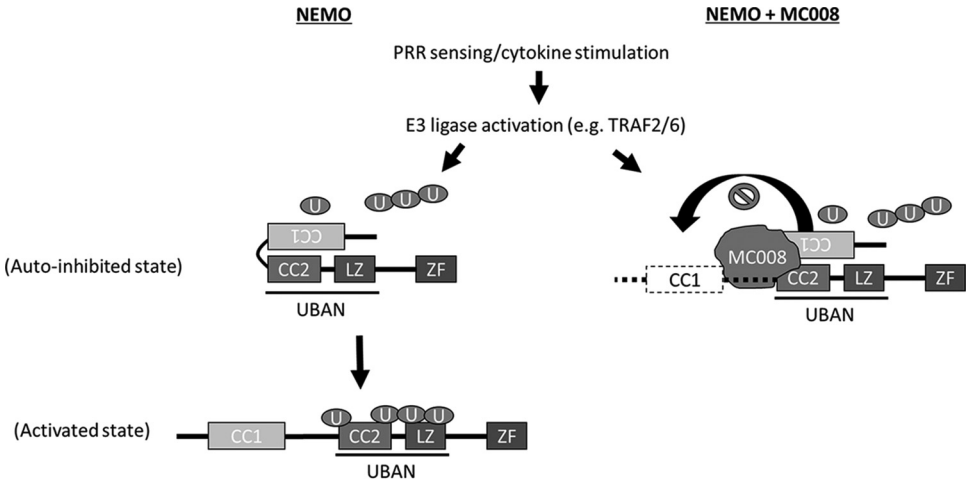

FIG 6 Model of MC008 inhibition of NF-κB signaling. PRR and cytokine signaling pathways drive signal transduction leading to the activation of E3 ligases such as TRAF proteins, which generate ubiquitin chains. NEMO is locked in an autoinhibited state by the CC1 domain until it is relieved by long ubiquitin chains binding to the UBAN domain. This binding event induces a conformational change, priming NEMO for downstream signaling. MC008 inhibits this ubiquitination event by binding to the CC1 and UBAN domains, thus preventing complex priming and downstream NF-κB signaling.

poxviral skin infections in humans and has been of long-standing interest (35–38). Well-characterized orthopoxviruses, like vaccinia virus, have long been known to produce broad arrays of inhibitors during infection that aggressively target NF-κB activation at various levels (7, 9). Although distantly related to, and highly divergent from, other types of poxviruses, molluscipoxviruses likely possess their own arrays of inhibitors that have evolved during their coevolution with humans.

Immune evasion by MCV may be partially attributable to the keratinocyte tropism of the virus and restricting infection to the upper layers of the epidermis (39). While the localization of the virus likely reduces interactions with the immune system to some extent, we and others have continued the process of systematically characterizing MCV-specific immunomodulatory proteins that target key elements of innate immune signaling pathways in this historically understudied virus. One factor restricting MCV research is the ongoing absence of animal and cell culture models of infection (40).

Nevertheless, we previously showed that MC132 recruits the p65 subunit of NF-κB to an E3 ligase complex, leading to its degradation by the proteasome, and that MC005 targets NEMO to prevent a priming event causing the disruption of downstream NF-κB activation (12, 14). Other researchers have shown that MC159 and MC160 are viral FLICE-like proteins that prevent TNF-induced apoptosis and inhibit IKKβ through binding to NEMO and degrading IKKα, respectively (15, 17, 41). MC163 was shown to inhibit apoptosis by preventing mitochondrial membrane permeabiliza-

TABLE 1 Comparison of three MCV proteins that target NEMO

	MCV protein		
Effect	**MC005[a]**	**MC008**	**MC159[b]**
Inhibits NEMO-NEMO interaction	No	No	Unknown
Region of NEMO interaction	2nd half of CC1/ before CC2	N and C termini	N-terminal residues 1–250
Inhibits NEMO-IKK interaction	No	No	Unknown
Inhibits NEMO monoubiquitination	No	Yes	No
Inhibits NEMO polyubiquitination	No	Yes	Yes
Inhibits NEMO activation after UBAN-ubiquitin activation	Yes	Yes	Unknown

[a]See reference 12.
[b]See references 15 and 16.

tion (42). MC080 was shown to disrupt major histocompatibility complex class I antigen presentation by targeting tapasin, a component of the peptide-loading complex, for ubiquitination and subsequent degradation (13). Despite this progress, likely many more inhibitors remain to be identified in the MCV genome.

PRRs of the innate immune system, such as cytosolic nucleic acid sensors and TLRs, are a crucial means of detecting invading viral pathogens, leading to type I IFN activation. This coupled with the production of proinflammatory cytokines such as IL-1β and TNF, which induce potent inflammatory signaling, help orchestrate the emergence of an adaptive immune response, resulting in virus clearance (34). Similar to our previous observations for MC005 and MC132, MC008 inhibited PRR- and inflammatory cytokine-induced NF-κB activation and proinflammatory cytokine production. Furthermore, it did not perturb IRF activation in any of these pathways or Ras-Elk1 control pathway activation.

Using a process of sequential activation of key signaling pathway components, we mapped the effect of MC008 on the IKK complex. We found that it specifically interacted with the core regulatory component of the IKK complex, NEMO, which translates upstream ubiquitin-generating stimuli into the activation of the associated IKKs and, thus, the activation of NF-κB. Given that the IKK complex plays a central regulatory role in inflammatory signaling and multiple pathways converge at this point, elements of this complex are common targets for viruses seeking to evade and subvert the immune response (8, 43).

While our knowledge of the IKK complex advances, a precise understanding of its multilayered mechanism of activation is continually emerging. However, it is clear that ubiquitination plays a key role in this process. Following upstream activation by various stimuli, E3 ligases such as TRAF2, TRAF6, cellular inhibitor of apoptosis protein (cIAP), and the LUBAC complex produce ubiquitin chains that bind to NEMO, among other signaling proteins (44, 45). K63-linked ubiquitin chains that bind to NEMO serve as a scaffold to bring proteins such as the TAB/TAK complex into the proximity of IKKα/β, thus enabling their phosphorylation (46). Furthermore, both K63-linked and Met-1-linked ubiquitin chains induce conformational changes in the IKK complex that allow this phosphorylation event to occur, ultimately leading to the release of NF-κB for nuclear translocation (5, 30, 31). Since ubiquitin binding is a requirement for NEMO activation, we used a NEMO K277A mutant, which has a point mutation that simulates a ubiquitin-bound state, as previously described (12). Interestingly, MC008, like MC005, potently inhibited the activation of NF-κB by this constitutively active form of NEMO.

We used a truncation-based approach to determine the region of NEMO required for the MC008 interaction. The MC008 interaction was maintained across all truncations. However, there was a reduced association with a truncation lacking the coiled-coil 1 (CC1) domain, suggesting that this region is important for its inhibition. MC008 binding to this region does not impair NEMO dimerization or its ability to associate with IKKα or IKKβ. However, we observed significant reductions in NEMO monoubiquitination and polyubiquitination when MC008 was introduced. The CC1 domain of NEMO has been shown to be a common target of MCV proteins; MC159 was previously shown to competitively bind to the NEMO N-terminal region (positions 1 to 250), which contains this CC1 domain, and to prevent cIAP1 polyubiquitination of NEMO (16).

We previously demonstrated that MC005 interacts with the CC1 domain of NEMO and prevents an important ubiquitin-induced conformational change required for downstream signaling (12). The beginning of the CC1 domain interacts with the C termini of IKK proteins (4, 47). This domain has also been shown to autoinhibit NEMO in its resting state by preventing ubiquitin binding to the ubiquitin binding in ABIN and NEMO (UBAN) domain, and this resting state is overcome only by long ubiquitin chains (48). The CC2 domain and leucine zipper form this UBAN domain. This region also regulates the conformational change that allows the phosphorylation of IKKβ by TAK1 on serines 177 and 181 in the activation loop, leading to IKK activation (5, 49). The

C-terminal zinc finger has also been shown to be another ubiquitin binding domain (50). Given that MC008 maintains the ability to interact with multiple NEMO domains and that it potently inhibits both early and late ubiquitination, we propose that MC008 binding to NEMO prevents ubiquitin chains from disrupting its autoinhibited state, thereby preventing ubiquitin-UBAN domain interactions (Fig. 6). Thus, as for MC005, not only does this research further elaborate how MCV inhibits inflammation, it also helps to confirm models of IKK complex regulation.

One perplexing aspect of the data is that MC008 inhibits both IKKα/β and p65 phosphorylation, with only a minor delay in IκBα degradation. In the canonical pathway, fully activated IKKβ phosphorylates IκBα on serines 32 and 36, triggering its degradation (51). However, the IKKβ-mediated regulation of p65 by phosphorylation is more complex. During signaling, p65 is potentially phosphorylated on 11 known sites (52), controlling conformational changes, protein-protein interactions, and stability. IKKβ is associated with at least two of these, serine 536 (53–57) and serine 468 (58). While we observed that MC008 inhibited serine 536 phosphorylation, we did not detect serine 468 phosphorylation in TNF-α-stimulated HEK293T cells (data not shown). We propose that MC008 may inhibit IKK complex activation in a specific manner that targets the regulation of p65 without a potent effect on IκBα regulation. We are now investigating the precise nature of this difference, which may give new insights into previously uncharacterized nuances of NEMO-induced IKK activation in NF-κB regulation.

Our investigation into MCV ORFs that disrupt inflammatory signaling revealed that MC008 potently inhibits PRR- and cytokine-induced NF-κB signaling. We describe a precise mechanism by which MC008 targets signaling within the known model of IKK complex regulation. Previously, MC005, MC132, MC159, and MC160 have been described as inhibitors of NF-κB signaling, with MC008 adding to this class of MCV inhibitors. By specifically targeting NEMO in a variety of ways, viruses like MCV appear to have heavily invested in evolving the capacity to efficiently inhibit its activation. In doing so, these viruses perturb the viral sensing-induced production of both type I interferon and proinflammatory cytokines and the activity of the latter in infected cells.

Further investigation of the MCV genome will likely reveal more inhibitors of innate immune signaling, which will expand our understanding of this fascinating virus while offering novel insights into innate signaling pathways and potential new avenues for therapeutic intervention in human inflammatory disease.

MATERIALS AND METHODS

Cell culture techniques. HEK293T, HeLa, and HaCaT cells were cultured in Dulbecco's modified Eagle medium (DMEM) (catalog number 61965-026; Gibco) supplemented with 10% fetal bovine serum (catalog number F9665; Sigma) and containing 1% penicillin-streptomycin (catalog number 15140-122; Gibco). Cells were subsequently washed with sterile phosphate-buffered saline (PBS) and detached from the flask by the addition of prewarmed 0.05% or 0.25% trypsin-EDTA. For cell stimulations, 50 ng/mL TNF-α (catalog number 570104; BioLegend) or 1 μg/mL poly(dA-dT) (catalog number P0883; Sigma) was used.

Plasmids and oligonucleotides. Custom-synthesized MCV subtype 1 MC008L (GenScript) was subcloned into the KpnI and NotI sites of the pCEP4 plasmid (catalog number V04450; Invitrogen) containing a C-terminal FLAG (DYKDDDDK) or HA (YPYDVPDYA) tag. MC008L was also cloned into these sites in the pMEP4 plasmid with a FLAG tag for $CdCl_2$-inducible expression. All other plasmids were sourced as described previously (12, 14).

Reporter gene assays. HEK293T cells were seeded at 2×10^5 cells/mL in a flat-bottomed 96-well plate with 200 μL of DMEM/well. The cells were transfected 16 h later using Gene Juice transfection reagent (catalog number 70967; Merck Millipore) with 80 ng of the luciferase reporter gene, 40 ng of pGL3-Renilla luciferase, and the indicated quantities of the expression vector. The concentration of these constructs was adjusted to give a final volume of 220 ng of DNA/well using empty vector pCMV-HA. After 24 h, the cells were either stimulated with cytokines or directly lysed using passive lysis buffer (25 mM Tris-phosphate [pH 7.8], 2 mM dithiothreitol [DTT], 2 mM 1,2-diaminocyclohexane *N*,*N*,*N*′,*N*′-tetraacetic acid, 10% glycerol, 1% Triton X-100) as described in reference 59. Twenty microliters of the lysates was added to two identical white microplates, and the luciferase assay substrate [20 mM Tricine, 2.67 mM $MgSO_4 \cdot 7H_2O$, 0.1 mM EDTA, 33.3 mM DTT, 530 μM ATP, 270 μM acetyl coenzyme A sodium salt, 420 nM D-luciferin, 5 μM NaOH, 9.7 mM $(MgCO_3)_4Mg(OH)_2 \cdot 5H_2O$] and coelenterazine (catalog number 10110-1; Biotium Inc.) were added to induce the light-emitting reaction. The lysates were then analyzed using a Thermo Scientific Luminoskan microplate luminometer with Ascent software v2.6. The transfection efficiency was controlled by normalizing firefly

luciferase activity to *Renilla* luciferase activity. For the Elk1 reporter assay, the pathway was driven by the RasVHa expression vector, 1 ng of the pFA-Elk1 expression vector, and 80 ng of the pFR-luciferase reporter plasmid.

Antibodies. Anti-β-actin (catalog number A5316; Sigma-Aldrich), anti-FLAG (M2) (catalog number F3165; Sigma-Aldrich), and anti-HA (catalog number 901515; BioLegend) were the primary antibodies used for immunoblotting. The secondary antibodies used for immunoblotting were IRDye 680LT anti-mouse (catalog number 926-68070; Li-Cor) and IRDye 800CW anti-rabbit (catalog number 926-32211; Li-Cor). The following other antibodies were used: anti-IκBα (catalog number 4814; Cell Signaling Technology [CST]), anti-phospho-p65 (clone 93H1) (CST), anti-p65 (clone D14E12) (CST), phospho-IKKα/β (Ser176/180) (clone 16A6) rabbit monoclonal (CST), and anti-NEMO (catalog number 2685; CST).

ELISA. Cell culture supernatants were harvested and assayed for IL-6 using an enzyme-linked immunosorbent assay (ELISA) kit (catalog number DY206; R&D Systems) according to the manufacturer's protocol.

Immunoblotting. Cells were seeded at 6×10^5 cells per well in 6-well plates and transfected with 4 μg/well of the plasmid 16 h later using Gene Juice transfection reagent (Merck Millipore). After 24 h, the cells were lysed using 200 μL of sample buffer with 100 mM dithiothreitol (catalog number 10592945; Fisher Scientific) and 1 μL/mL of Benzonase (catalog number 70746-3; Merck Millipore), as previously described (12). Lysates were left on ice for 5 min and then boiled at 100°C for 5 min. Twenty microliters of the lysates was then loaded onto 8 to 20% resolving gels, and SDS-PAGE was performed. The separated proteins were then transferred onto a nitrocellulose membrane (catalog number 15259804; Fisher Scientific) and blocked with 3% (wt/vol) bovine serum albumin (BSA) and 0.1% (vol/vol) Tween 20 in PBS for 1 h. The membrane was then probed with primary antibody (diluted 1:1,000 for HA, 1:5,000 for FLAG, and 1:10,000 for β-actin in blocking buffer) overnight at 4°C on a tube roller. The membrane was subsequently washed in PBS with 0.1% Tween 20 three times for 5 min and incubated with the secondary antibody at room temperature for 1 h, before washing a further three times. The membranes were then viewed using the Odyssey B446 imaging system (Li-Cor Biosciences) and analyzed with Image Studio Lite software v5.2 (Li-Cor Biosciences).

Immunoprecipitation. Cells were seeded at 4×10^6 cells/10-cm dish and transfected 16 h later using Gene Juice transfection reagent (Merk Millipore). Cells were then lysed on ice with ice-cold lysis buffer (50 mM Tris [pH 7.4], 150 mM NaCl, 0.5% [vol/vol] NP-40, 30 mM NaF, 5 mM EDTA, 10% [vol/vol] glycerol, and 40 mM β-glycerophosphate containing the inhibitors 1 mM Na_3VO_4, 1 mM phenylmethylsulfonyl fluoride, and 1% [vol/vol] aprotinin), as described previously (12). Lysates were cleared by centrifugation for 10 min at 4°C and transferred into precooled Eppendorf tubes on ice. Ten microliters of anti-FLAG M2 affinity gel (catalog number A2220; Sigma) per plate was centrifuged and washed three times with lysis buffer to equilibrate the beads. These were added to the cleared lysates and left rolling overnight at 4°C. The beads were then washed three times with 1 mL of ice-cold lysis buffer. Four microliters (from a 5-mg/mL stock) of reconstituted 3×FLAG peptide (catalog number F3290; Sigma) and 80 μL of PBS were added to each sample, and the samples were left rolling at 4°C for 30 min to elute the immunoprecipitated material. The samples were then separated from the beads, 40 μL of sample buffer was added to each sample, and the samples were subsequently immunoblotted for the indicated proteins.

Generation of MC008-expressing stable cell lines. Doxycycline-inducible stable cell generation was performed by employing the pLVX-TetOne-Puro expression construct with the cloning of MC008L into the EcoRI and AgeI sites. Lentivirus was packaged with the Lenti-X Tet-One inducible expression system (TaKaRa), as described in the manual. Cells were selected with 5 μg/mL puromycin. Episomally stable pMEP4-MC008 cells were transfected with 8 μg plasmid pMEP4-MC008, selected with 300 μg/mL hygromycin (Sigma) for 1 week, and maintained in 100 μg/mL hygromycin.

Confocal microscopy. Cells were seeded at 7×10^4 cells/well onto 8-well chamber slides (catalog number 1626066; Fisher Scientific) and transfected 16 h later. The next day, cells were washed in PBS and fixed with 4% (wt/vol) paraformaldehyde for 12 min. Cells were then permeabilized for 15 min with 0.5% (wt/vol) Triton X-100 in PBS and blocked for 1 h in 5% (wet/vol) BSA–0.05% (vol/vol) Tween 20 in PBS. Cells were incubated overnight with anti-FLAG Alexa Fluor 488 (catalog number MA1-142-A488; Fisher Scientific) and anti-HA Alexa Fluor 647 (catalog number 26183-A647; Fisher Scientific) at 1:2,000 and 1:500 in blocking solution, respectively. The slides were subsequently washed with PBS–0.05% Tween 20 and mounted with ProLong gold antifade mountant with 4′,6-diamidino-2-phenylindole (DAPI) (catalog number P36931; Invitrogen). Images were obtained with a Lecia SP8 confocal microscope with a 40× oil immersion objective.

Statistical analysis. The data obtained from triplicate experiments are presented as the means ± standard deviations. Mean differences were compared to the positive control using two-way analysis of variance (ANOVA) with correction for multiple comparisons using Dunnett's test in GraphPad Prism software. Statistical significance is indicated by asterisks in the figures (*, $P < 0.05$; **, $P < 0.01$; ***, $P < 0.001$; ****, $P < 0.0001$).

Data availability. The data used in this study are available in the Figshare open data repository. Immunoblots are available at https://doi.org/10.6084/m9.figshare.22149293. Numerical data are available at https://doi.org/10.6084/m9.figshare.22149029.

ACKNOWLEDGMENTS

This work was funded by Science Foundation Ireland (SFI) grant number 19/FFP/6848.

We declare no conflict of interest.

REFERENCES

1. Christensen MH, Paludan SR. 2017. Viral evasion of DNA-stimulated innate immune responses. Cell Mol Immunol 14:4–13. https://doi.org/10.1038/cmi.2016.06.
2. Gürtler C, Bowie AG. 2013. Innate immune detection of microbial nucleic acids. Trends Microbiol 21:413–420. https://doi.org/10.1016/j.tim.2013.04.004.
3. Adhikari A, Xu M, Chen ZJ. 2007. Ubiquitin-mediated activation of TAK1 and IKK. Oncogene 26:3214–3226. https://doi.org/10.1038/sj.onc.1210413.
4. Barczewski AH, Ragusa MJ, Mierke DF, Pellegrini M. 2019. The IKK-binding domain of NEMO is an irregular coiled coil with a dynamic binding interface. Sci Rep 9:2950. https://doi.org/10.1038/s41598-019-39588-2.
5. Rahighi S, Ikeda F, Kawasaki M, Akutsu M, Suzuki N, Kato R, Kensche T, Uejima T, Bloor S, Komander D, Randow F, Wakatsuki S, Dikic I. 2009. Specific recognition of linear ubiquitin chains by NEMO is important for NF-kappaB activation. Cell 136:1098–1109. https://doi.org/10.1016/j.cell.2009.03.007.
6. Perkins ND. 2000. The Rel/NF-kappa B family: friend and foe. Trends Biochem Sci 25:434–440. https://doi.org/10.1016/s0968-0004(00)01617-0.
7. Lu Y, Zhang L. 2020. DNA-sensing antiviral innate immunity in poxvirus infection. Front Immunol 11:1637. https://doi.org/10.3389/fimmu.2020.01637.
8. Phelan T, Little MA, Brady G. 2020. Targeting of the cGAS-STING system by DNA viruses. Biochem Pharmacol 174:113831. https://doi.org/10.1016/j.bcp.2020.113831.
9. Brady G, Bowie AG. 2014. Innate immune activation of NFκB and its antagonism by poxviruses. Cytokine Growth Factor Rev 25:611–620. https://doi.org/10.1016/j.cytogfr.2014.07.004.
10. van der Wouden JC, van der Sande R, Kruithof EJ, Sollie A, van Suijlekom-Smit LW, Koning S. 2017. Interventions for cutaneous molluscum contagiosum. Cochrane Database Syst Rev 5:CD004767. https://doi.org/10.1002/14651858.CD004767.pub4.
11. Senkevich TG, Koonin EV, Bugert JJ, Darai G, Moss B. 1997. The genome of molluscum contagiosum virus: analysis and comparison with other poxviruses. Virology 233:19–42. https://doi.org/10.1006/viro.1997.8607.
12. Brady G, Haas DA, Farrell PJ, Pichlmair A, Bowie AG. 2017. Molluscum contagiosum virus protein MC005 inhibits NF-κB activation by targeting NEMO-regulated IκB kinase activation. J Virol 91:e00545-17. https://doi.org/10.1128/JVI.00545-17.
13. Harvey IB, Wang X, Fremont DH. 2019. Molluscum contagiosum virus MC80 sabotages MHC-I antigen presentation by targeting tapasin for ER-associated degradation. PLoS Pathog 15:e1007711. https://doi.org/10.1371/journal.ppat.1007711.
14. Brady G, Haas DA, Farrell PJ, Pichlmair A, Bowie AG. 2015. Poxvirus protein MC132 from molluscum contagiosum virus inhibits NF-κB activation by targeting p65 for degradation. J Virol 89:8406–8415. https://doi.org/10.1128/JVI.00799-15.
15. Randall CMH, Jokela JA, Shisler JL. 2012. The MC159 protein from the molluscum contagiosum poxvirus inhibits NF-κB activation by interacting with the IκB kinase complex. J Immunol 188:2371–2379. https://doi.org/10.4049/jimmunol.1100136.
16. Biswas S, Shisler JL. 2017. Molluscum contagiosum virus MC159 abrogates cIAP1-NEMO interactions and inhibits NEMO polyubiquitination. J Virol 91:e00276-17. https://doi.org/10.1128/JVI.00276-17.
17. Nichols DB, Shisler JL. 2009. Poxvirus MC160 protein utilizes multiple mechanisms to inhibit NF-kappaB activation mediated via components of the tumor necrosis factor receptor 1 signal transduction pathway. J Virol 83:3162–3174. https://doi.org/10.1128/JVI.02009-08.
18. Tang Q, Chakraborty S, Xu G. 2018. Mechanism of vaccinia viral protein B14-mediated inhibition of IκB kinase β activation. J Biol Chem 293:10344–10352. https://doi.org/10.1074/jbc.RA118.002817.
19. DiPerna G, Stack J, Bowie AG, Boyd A, Kotwal G, Zhang Z, Arvikar S, Latz E, Fitzgerald KA, Marshall WL. 2004. Poxvirus protein N1L targets the I-kappaB kinase complex, inhibits signaling to NF-kappaB by the tumor necrosis factor superfamily of receptors, and inhibits NF-kappaB and IRF3 signaling by Toll-like receptors. J Biol Chem 279:36570–36578. https://doi.org/10.1074/jbc.M400567200.
20. Ember SWJ, Ren H, Ferguson BJ, Smith GL. 2012. Vaccinia virus protein C4 inhibits NF-κB activation and promotes virus virulence. J Gen Virol 93:2098–2108. https://doi.org/10.1099/vir.0.045070-0.
21. Rahman MM, Mohamed MR, Kim M, Smallwood S, McFadden G. 2009. Co-regulation of NF-kappaB and inflammasome-mediated inflammatory responses by myxoma virus pyrin domain-containing protein M013. PLoS Pathog 5:e1000635. https://doi.org/10.1371/journal.ppat.1000635.
22. Diel DG, Delhon G, Luo S, Flores EF, Rock DL. 2010. A novel inhibitor of the NF-κB signaling pathway encoded by the parapoxvirus Orf virus. J Virol 84:3962–3973. https://doi.org/10.1128/JVI.02291-09.
23. Fang R, Wang C, Jiang Q, Lv M, Gao P, Yu X, Mu P, Zhang R, Bi S, Feng J-M, Jiang Z. 2017. NEMO-IKKβ are essential for IRF3 and NF-κB activation in the cGAS-STING pathway. J Immunol 199:3222–3233. https://doi.org/10.4049/jimmunol.1700699.
24. Ablasser A, Schmid-Burgk JL, Hemmerling I, Horvath GL, Schmidt T, Latz E, Hornung V. 2013. Cell intrinsic immunity spreads to bystander cells via the intercellular transfer of cGAMP. Nature 503:530–534. https://doi.org/10.1038/nature12640.
25. Valentine R, Smith GL. 2010. Inhibition of the RNA polymerase III-mediated dsDNA-sensing pathway of innate immunity by vaccinia virus protein E3. J Gen Virol 91:2221–2229. https://doi.org/10.1099/vir.0.021998-0.
26. Kawasaki T, Kawai T. 2014. Toll-like receptor signaling pathways. Front Immunol 5:461. https://doi.org/10.3389/fimmu.2014.00461.
27. Park HH. 2018. Structure of TRAF family: current understanding of receptor recognition. Front Immunol 9:1999. https://doi.org/10.3389/fimmu.2018.01999.
28. Bloor S, Ryzhakov G, Wagner S, Butler PJG, Smith DL, Krumbach R, Dikic I, Randow F. 2008. Signal processing by its coil zipper domain activates IKK gamma. Proc Natl Acad Sci U S A 105:1279–1284. https://doi.org/10.1073/pnas.0706552105.
29. Polley S, Huang D-B, Hauenstein AV, Fusco AJ, Zhong X, Vu D, Schröfelbauer B, Kim Y, Hoffmann A, Verma IM, Ghosh G, Huxford T. 2013. A structural basis for IκB kinase 2 activation via oligomerization-dependent trans auto-phosphorylation. PLoS Biol 11:e1001581. https://doi.org/10.1371/journal.pbio.1001581.
30. Catici DA, Horne JE, Cooper GE, Pudney CR. 2015. Polyubiquitin drives the molecular interactions of the NF-κB essential modulator (NEMO) by allosteric regulation. J Biol Chem 290:14130–14139. https://doi.org/10.1074/jbc.M115.640417.
31. Emmerich CH, Ordureau A, Strickson S, Arthur JSC, Pedrioli PGA, Komander D, Cohen P. 2013. Activation of the canonical IKK complex by K63/M1-linked hybrid ubiquitin chains. Proc Natl Acad Sci U S A 110:15247–15252. https://doi.org/10.1073/pnas.1314715110.
32. Hinz M, Stilmann M, Arslan SÇ, Khanna KK, Dittmar G, Scheidereit C. 2010. A cytoplasmic ATM-TRAF6-cIAP1 module links nuclear DNA damage signaling to ubiquitin-mediated NF-κB activation. Mol Cell 40:63–74. https://doi.org/10.1016/j.molcel.2010.09.008.
33. Rahighi S, Iyer M, Oveisi H, Nasser S, Duong V. 2022. Structural basis for the simultaneous recognition of NEMO and acceptor ubiquitin by the HOIP NZF1 domain. Sci Rep 12:12241. https://doi.org/10.1038/s41598-022-16193-4.
34. Yu H, Bruneau RC, Brennan G, Rothenburg S. 2021. Battle royale: innate recognition of poxviruses and viral immune evasion. Biomedicines 9:765. https://doi.org/10.3390/biomedicines9070765.
35. Meza-Romero R, Navarrete-Dechent C, Downey C. 2019. Molluscum contagiosum: an update and review of new perspectives in etiology, diagnosis, and treatment. Clin Cosmet Investig Dermatol 12:373–381. https://doi.org/10.2147/CCID.S187224.
36. Lu B, Cui L-B, Gu M-H, Shi C, Sun C-W, Zhao K-C, Bi J, Tan Z-M, Guo X-L, Huo X, Bao C-J. 2019. Outbreak of vaccinia virus infection from occupational exposure, China, 2017. Emerg Infect Dis 25:1192–1195. https://doi.org/10.3201/eid2506.171306.
37. Chen X, Anstey AV, Bugert JJ. 2013. Molluscum contagiosum virus infection. Lancet Infect Dis 13:877–888. https://doi.org/10.1016/S1473-3099(13)70109-9.
38. Kaler J, Hussain A, Flores G, Kheiri S, Desrosiers D. 2022. Monkeypox: a comprehensive review of transmission, pathogenesis, and manifestation. Cureus 14:e26531. https://doi.org/10.7759/cureus.26531.
39. Shisler JL. 2015. Immune evasion strategies of molluscum contagiosum virus. Adv Virus Res 92:201–252. https://doi.org/10.1016/bs.aivir.2014.11.004.
40. Mendez-Rios JD, Yang Z, Erlandson KJ, Cohen JI, Martens CA, Bruno DP, Porcella SF, Moss B. 2016. Molluscum contagiosum virus transcriptome in abortively infected cultured cells and a human skin lesion. J Virol 90:4469–4480. https://doi.org/10.1128/JVI.02911-15.
41. Shisler JL. 2014. Viral and cellular FLICE-inhibitory proteins: a comparison of their roles in regulating intrinsic immune responses. J Virol 88:6539–6541. https://doi.org/10.1128/JVI.00276-14.
42. Coutu J, Ryerson MR, Bugert J, Brian Nichols D. 2017. The molluscum contagiosum virus protein MC163 localizes to the mitochondria and dampens mitochondrial mediated apoptotic responses. Virology 505:91–101. https://doi.org/10.1016/j.virol.2017.02.017.

43. Amaya M, Keck F, Bailey C, Narayanan A. 2014. The role of the IKK complex in viral infections. Pathog Dis 72:32–44. https://doi.org/10.1111/2049-632X.12210.
44. Dhillon B, Aleithan F, Abdul-Sater Z, Abdul-Sater AA. 2019. The evolving role of TRAFs in mediating inflammatory responses. Front Immunol 10:104. https://doi.org/10.3389/fimmu.2019.00104.
45. Rittinger K, Ikeda F. 2017. Linear ubiquitin chains: enzymes, mechanisms and biology. Open Biol 7:170026. https://doi.org/10.1098/rsob.170026.
46. Jun JC, Kertesy S, Jones MB, Marinis JM, Cobb BA, Tigno-Aranjuez JT, Abbott DW. 2013. Innate immune-directed NF-κB signaling requires site-specific NEMO ubiquitination. Cell Rep 4:352–361. https://doi.org/10.1016/j.celrep.2013.06.036.
47. Sebban H, Yamaoka S, Courtois G. 2006. Posttranslational modifications of NEMO and its partners in NF-kappaB signaling. Trends Cell Biol 16:569–577. https://doi.org/10.1016/j.tcb.2006.09.004.
48. Hauenstein AV, Xu G, Kabaleeswaran V, Wu H. 2017. Evidence for M1-linked polyubiquitin-mediated conformational change in NEMO. J Mol Biol 429:3793–3800. https://doi.org/10.1016/j.jmb.2017.10.026.
49. Wang C, Deng L, Hong M, Akkaraju GR, Inoue J, Chen ZJ. 2001. TAK1 is a ubiquitin-dependent kinase of MKK and IKK. Nature 412:346–351. https://doi.org/10.1038/35085597.
50. Cordier F, Grubisha O, Traincard F, Véron M, Delepierre M, Agou F. 2009. The zinc finger of NEMO is a functional ubiquitin-binding domain. J Biol Chem 284:2902–2907. https://doi.org/10.1074/jbc.M806655200.
51. Brown K, Gerstberger S, Carlson L, Franzoso G, Siebenlist U. 1995. Control of I kappa B-alpha proteolysis by site-specific, signal-induced phosphorylation. Science 267:1485–1488. https://doi.org/10.1126/science.7878466.
52. Christian F, Smith EL, Carmody RJ. 2016. The regulation of NF-κB subunits by phosphorylation. Cells 5:12. https://doi.org/10.3390/cells5010012.
53. Buss H, Dörrie A, Schmitz ML, Hoffmann E, Resch K, Kracht M. 2004. Constitutive and interleukin-1-inducible phosphorylation of p65 NF-kappaB at serine 536 is mediated by multiple protein kinases including IkappaB kinase (IKK)-alpha, IKKbeta, IKKepsilon, TRAF family member-associated (TANK)-binding kinase 1 (TBK1), and an unknown kinase and couples p65 to TATA-binding protein-associated factor II31-mediated interleukin-8 transcription. J Biol Chem 279:55633–55643. https://doi.org/10.1074/jbc.M409825200.
54. Sakurai H, Chiba H, Miyoshi H, Sugita T, Toriumi W. 1999. IkappaB kinases phosphorylate NF-kappaB p65 subunit on serine 536 in the transactivation domain. J Biol Chem 274:30353–30356. https://doi.org/10.1074/jbc.274.43.30353.
55. Sizemore N, Lerner N, Dombrowski N, Sakurai H, Stark GR. 2002. Distinct roles of the Ikappa B kinase alpha and beta subunits in liberating nuclear factor kappa B (NF-kappa B) from Ikappa B and in phosphorylating the p65 subunit of NF-kappa B. J Biol Chem 277:3863–3869. https://doi.org/10.1074/jbc.M110572200.
56. Haller D, Russo MP, Sartor RB, Jobin C. 2002. IKK beta and phosphatidylinositol 3-kinase/Akt participate in non-pathogenic Gram-negative enteric bacteria-induced RelA phosphorylation and NF-kappa B activation in both primary and intestinal epithelial cell lines. J Biol Chem 277:38168–38178. https://doi.org/10.1074/jbc.M205737200.
57. Yoboua F, Martel A, Duval A, Mukawera E, Grandvaux N. 2010. Respiratory syncytial virus-mediated NF-κB p65 phosphorylation at serine 536 is dependent on RIG-I, TRAF6, and IKKβ. J Virol 84:7267–7277. https://doi.org/10.1128/JVI.00142-10.
58. Schwabe RF, Sakurai H. 2005. IKKbeta phosphorylates p65 at S468 in transactivaton [*sic*] domain 2. FASEB J 19:1758–1760. https://doi.org/10.1096/fj.05-3736fje.
59. Promega. 2015. Luciferase assay system technical bulletin. https://www.promega.com/-/media/files/resources/protocols/technical-bulletins/0/luciferase-assay-system-protocol.pdf.